Synchrotron radiation photoemission study of Yb-intercalated C_{60}

Shao-Long He, Hong-Nian Li,* Xiao-Xiong Wang, Hai-Yang Li, Ya-Bo Xu, and Shi-Ning Bao
Department of Physics, Zhejiang University, Hangzhou 310027, People's Republic of China

Kurash Ibrahim, Hai-Jie Qian, Run Su, Jun Zhong, Cai-Hao Hong, and M. I. Abbas
Laboratory of Synchrotron Radiation, Institute of High Energy Physics, Chinese Academy of Sciences, Beijing 100039, People's Republic of China

(Received 18 May 2004; revised manuscript received 27 September 2004; published 4 February 2005)

The valence band evolution of C_{60} film upon Yb intercalation is investigated by the synchrotron radiation photoemission spectroscopy (SR-PES) technique. The results show that only $Yb_{2.75}C_{60}$ forms at lower intercalation stages and imply that other phases of Yb_xC_{60} ($x>2.75$) form with more Yb atoms intercalated into the $Yb_{2.75}C_{60}$ sample. No Fermi edge is observed for all the spectral lines in this work, which reveals that the superconducting Yb fulleride, whether it is $Yb_{2.75}C_{60}$ or other phase, has semiconducting property at room temperature. To extract the intrinsic density of state of the valence band from the Yb $4f$-superposed experimental data, the SR-PE spectra were measured for the well-defined phase of $Yb_{2.75}C_{60}$ with varying photon energies (18.0–45.0 eV). The results show that the spectral data can drastically depart from the density of states of the valence band due to the photoemission of Yb $4f$ core levels. However, the valence band can still be quantitatively extracted from the experimental data by the least-square simulation.

DOI: 10.1103/PhysRevB.71.085404 PACS number(s): 73.20.At, 71.20.Tx, 73.61.Wp

I. INTRODUCTION

Alkali and alkaline-earth-intercalated C_{60} solids have been studied intensively in the past decade due to the superconducting transitions at relatively high temperatures.[1,2] A great deal of attention is now dedicated to the rare-earth-intercalated fullerides, mainly due to the observations of superconductivity,[3,4] ferromagnetism and giant magnetoresistance.[5–7] Electronic structure is the foundation of understanding the novel properties of rare-earth fullerides. However, there are many fewer reported results concerning the electronic structure as compared to the alkali and alkaline-earth fillerides. In this paper, we report the synchrotron radiation ultraviolet photoemission spectroscopy (SR-UPS) of Yb-intercalated C_{60} thin film.

A previous ultraviolet photoemission study[8] exhibited the semiconducting property of $Yb_{2.75}C_{60}$ at room temperature. If $Yb_{2.75}C_{60}$ is indeed the superconducting phase as proposed by Özdas *et al.*,[3] it is the first finding of superconducting fulleride with semiconducting property at room temperature. For comparison, alkali-doped superconducting A_3C_{60} (A=K,Rb) (Refs. 1 and 9) exhibited metal-like photoemissions.[10–13] Alkaline-earth-doped superconducting Ca_5C_{60}, Sr_6C_{60} [actually Sr_4C_{60} (Refs. 14 and 15)] and Ba_6C_{60} [actually Ba_4C_{60} (Refs. 14 and 15)] were also metallic or semimetallic in normal states.[16–22] However, the superconducting phase of $Yb_{2.75}C_{60}$ was questioned by Takeuchi *et al.*[23] although the superconducting transition did exist in the Yb intercalated fullerides.[3,23] Some other reports[24,25] seem to support the idea of Takeuchi *et al.*[23] In this paper, we investigate the valence evolution of C_{60} thin film from pure C_{60} to Yb saturation by the SR-UPS measurements. The results exhibit the semiconducting properties for all the phases. Thus the semiconducting property at room temperature for the superconducting Yb fulleride is revealed, whether the superconducting phase is $Yb_{2.75}C_{60}$ (Ref. 3) or Yb_4C_{60}.[23]

The $4f$ electrons of rare-earth metal generally distribute very near the Fermi level and the photoionization cross sections are relatively large in the photon energy region where the UPS is carried out. The contribution of Yb $4f$ electrons to the UPS result should be subtracted to obtain a precise knowledge of the valance band structure of Yb fulleride. In Sec. III, we measure the UPS of $Yb_{2.75}C_{60}$ with varying photon energies. $Yb_{2.75}C_{60}$ is the unique well-defined phase of Yb fulleride up to date.[3,8,26] The valence state of Yb is divalent in this phase.[26,27] Within the photon energy region (from 18 to 45 eV) used in this work, the photoinization cross section increases for Yb $4f$ and decreases for C $2p$ with the increasing photon energies.[28] Thus we have the opportunity to deduce quantitatively the components of the valence band and the $4f$ core levels in the measured UPS lines by spectral intensity simulations.

II. VALENCE BAND EVOLUTION OF C_{60} FILM UPON Yb INTERCALATION

A. Experiment

Sample preparations and measurements were performed in an ultrahigh vacuum system. The base pressure was 2×10^{-10} torr. The incident photons were induced from the 4B9B beam line of Beijing Synchrotron Radiation Facility. The overall energy resolution was 0.15–0.3 eV, depending on the photon energies. An angle-resolved spherical deflection analyzer was used to collect the photoelectrons at normal emission. For the polycrystalline sample, the angle-resolved UPS results should be considered to be analogous to the angle-integrated results. The UPS was measured with a sample bias of −5.0 V for the work function determination. Binding energy was referenced to the Fermi level of the Ag(111) substrate.

 ©2005 The American Physical Society

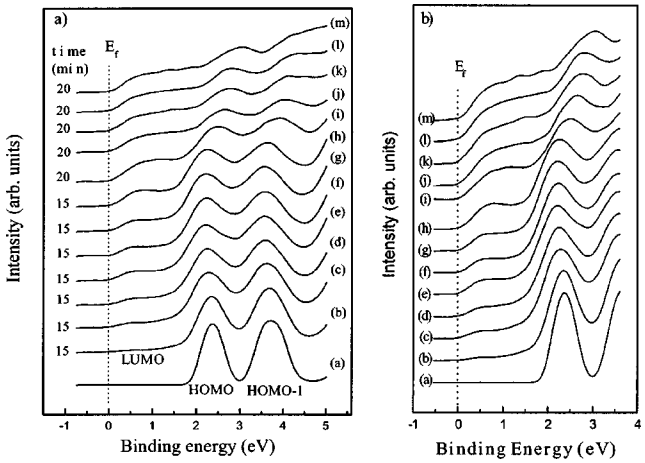

FIG. 1. (a) Valence-band evolution of Yb-intercalated C_{60} film. The bottom curve is the SR-UPS for pure C_{60} film. Spectral lines are normalized to the incident photon flux. (b) The enlarged view of the parts near the Fermi level, with the heights of HOMO features normalized to that of the pure C_{60} film. The intensity of the HOMO feature for pure C_{60} is multiplied by 1/2. The incident photon energy is 21.0 eV.

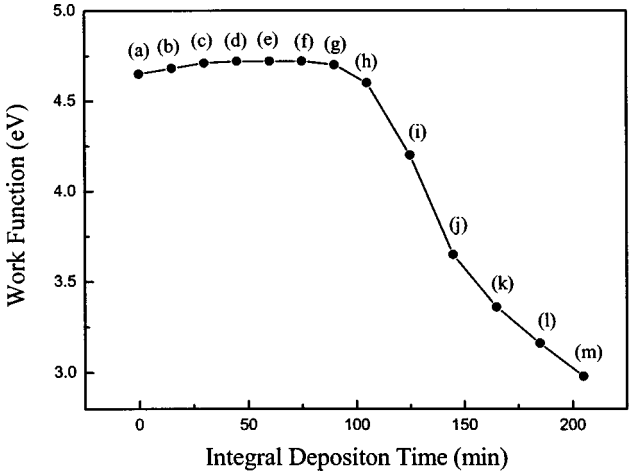

FIG. 2. Work functions (Φ) of the sample upon Yb intercalation. The values of Φ are determined by the second electron cutoffs of the spectral lines. The meaning of the symbols of (a), (b), *et al.* in the figure is the same as that in Fig. 1.

The Ag single crystal substrate was cleaned by cycles of Ar ion bombarding and annealing at ~550 °C until the clear (1×1) LEED pattern was observed and the C 1*s* and O 1*s* signals could not be observed by the x-ray photoemission (XPS) measurement. Thoroughly degassed C_{60} and Yb were sublimed from Ta boats located at about 11 cm from the Ag(111) surface. The C_{60} raw material was single crystals grown by the gas-phase method[29] that was ground into powder by using an agate mortar before filled into the Ta boat. The high-purity Yb (99.99%) was purchased from Beijing Research Institute for Nonferrous Metals.

A C_{60} film was first prepared by evaporating C_{60} molecules onto the substrate. The substrate was kept at room temperature during the C_{60} deposition. The film thickness is ~230 Å as determined by a quartz crystal oscillator. Then we evaporated Yb onto the C_{60} thin film. During the deposition of Yb, the sample was kept at 130±5 °C. The Yb doping procedure was carried out step by step. Once the deposition was over for each trail in the preparation chamber, the sample was transferred into the analyzer chamber for UPS measurement. The amount of Yb deposited onto the C_{60} film was controlled by the electric current through the Ta boat and the deposition time. We fixed the electric current at 9.0 A that was suitable for our experimental setup. With the deposition time of 15 or 20 min for each trail, Yb saturation occurred after more than 10 rounds of depositions.

B. Results and discussions

Figure 1 exhibits the valence band evolution from the pristine C_{60} film (bottom) to Yb saturation (top). The incident photon energy is 21.0 eV for all the SR-UPS lines. Curves in (a) are normalized to the incident photon flux. To emphasize the relative intensity of the lowest-unoccupied-molecular-orbital (LUMO) derived band, the spectral lines are normalized to the height of the highest-occupied-molecular-orbital (HOMO) derived band and redrawn in (b). The deposition time for each round is labeled next to the lines.

It is essential to show that the intercalation of Yb is saturated for the top line in Fig. 1 before we discuss the valence evolution. Figure 2 exhibits the work functions (Φ) of the sample upon the Yb intercalation. The work functions were determined by the second electron cutoffs. The value of Φ corresponding to the top line is ~2.9 eV that is near the work function (2.7–2.8 eV) of metal Yb.[30,31] Thus the results in Fig. 1 cover the electronic states for Yb fulleride from pristine C_{60} to Yb saturation.

By a minor amount of Yb deposition, the LUMO band in curve (b) and (c) is partially filled by the electron transfer from the Yb 6*s* orbital. HOMO and HOMO-1 move towards lower binding energy. The integral spectral intensity of the LUMO band increases continuously until curve (i) [or (j)] in Fig. 1(a), which indicates more electrons occupy the LUMO band with more Yb intercalation. The movement of the HOMO and HOMO-1 bands ceases at curve (c), and the positions of these bands keep unchanged until curve (g) as can be seen in Fig. 1(a) or more clearly in Fig. 1(b). Figure 2 exhibits the analogous variation of the work function. The work function of the sample increases slightly from curve (a) to (c), which may be due to the Fermi level alignment (pinning at the edge of the LUMO band) caused by the Yb doping. Then the work functions remain unchanged until curve (g). These observations coincide with the XPS (Ref. 32) and x-ray diffraction (XRD)[23] results that only $Yb_{2.75}C_{60}$ formed at lower doping stages. The samples corresponding to curve (b) through (g) are the mixtures of undoped C_{60} (or the solid solution) and $Yb_{2.75}C_{60}$. Curve (h) has a line shape very near to that of the phase-pure $Yb_{2.75}C_{60}$ (Ref. 8) characterized by the XPS measurement. However, the HOMO band of curve (h) moves slightly towards higher binding energy as compared to the HOMO band of curve (c) through (g). Thus we argue that the phase-pure $Yb_{2.75}C_{60}$ corresponds to the inter-

calation stage between curve (g) and (h). The work functions in Fig. 2 support the above ascription.

From curve (i) on, HOMO and HOMO-1 move obviously towards higher binding energy until curve (k) and the work function decreases substantially. The decrease of the work function can be interpreted either by the excess Yb atoms on the sample surface or the filling of the LUMO+1 band of C_{60}. However, the obvious movements of the HOMO band can only be explained by the LUMO+1 filling. With the LUMO+1 occupation, the Fermi level moves to the LUMO+1 band, and the LUMO feature together with the HOMO and HOMO-1 features moves to higher binding energies. The largest width of the combined LUMO and LUMO+1 bands is ~2.0 eV [curve (k) through (m)], which is nearly the same as that found in the alkaline-earth fullerides[16,17] where the LUMO+1 band was also filled.

UPS can detect only the top layer of fulleride samples.[33] Electronic structure at the surface may differ from that of the interior of the sample.[34] Thus it is desired to make clear whether the LUMO+1 filling occurs only at the surface or in the bulk of the sample. The sample thickness (230 Å) corresponds to ~28 layers of C_{60} by supposing a (111) surface termination of solid C_{60}. The number of the Yb layer should be ~56 for $Yb_{2.75}C_{60}$. The average distance between Yb ions in the plane parallel to the (111) surface is ~10 Å (the crystal structure of $Yb_{2.75}C_{60}$ is somewhat analogous with that of Rb_3C_{60} that was schematically shown in Ref. 34). (The departure from the vacancy centers of the Yb ions[27] is not related to the topics discussed here.) For metal Yb (fcc structured, lattice constant is 5.5 Å), the interatom distance is ~4 Å in the (111) plane. If Yb atoms did not diffuse into the sample after the uniform $Yb_{2.75}C_{60}$ sample formed, the atoms should accumulate on the surface from curve (g) [or (h)] on. The accumulated Yb should be ~20 layers for curve (m) according to the deposition time and the assumption of the (111) surface termination of Yb film. The UPS signal of $Yb_{2.75}C_{60}$ should be attenuated entirely, and the electronic structure of metal Yb (Ref. 8) should dominate the UPS line. However, curve (m) in Fig. 1 still exhibits the HOMO, LUMO, and LUMO+1 bands. Although it seems that there are excess Yb atoms on the sample surface for curve (m) by the inspection of the line shape and considering the work function, the amount of the excess atoms is far less than 20 layers. Thus we argue that Yb atoms can diffuse into the $Yb_{2.75}C_{60}$ sample and other fulleride phase(s) forms with the LUMO+1 band filling. It is difficult to determine the composition of the fullerides beyond $Yb_{2.75}C_{60}$ by the UPS technique. We speculate they might be Yb_4C_{60} (Ref. 23) and Yb_6C_{60} (Ref. 35) that were found by the XRD researches. It should be pointed out, however, Refs. 23 and 35 can only be considered as uncompleted and crude XRD studies on the stoichiometry of the Yb intercalated C_{60}. The topic of the phases of the Yb-intercalated fullerides is, in our opinion, still open.

In any case, there is no Fermi edge in all the spectral lines in Fig. 1. This observation reveals that the superconducting Yb fulleride is semiconducting at room temperature, whatever its stoichiometry is. Yb-intercalated C_{60} is the unique superconducting fulleride found so far with semiconduction-like photoemission at room temperature.

Although a semiconductor cannot directly transform to be a superconductor according to the contemporary physical concepts, the superconducting transition can occur for semiconductors with structural or electronic phase transitions. Arvanitidis *et al.*[24] recently found the electronic phase transition of $Sm_{2.75}C_{60}$ at 32 K. The valence state changed from 2+ to $(2+\varepsilon)$+ below 32 K, where ε is a positive quantity. If the electronic phase transition takes place also in Yb-intercalated C_{60}, the metallic state may emerge before the superconducting transition. Thus the result of this work cannot be considered as contradiction to basic physical concepts. On the contrary, by keeping in mind the strongly correlated electronic properties of rare-earth ions and C_{60}, our observations imply more interesting physical phenomena should be observed at low temperatures for Yb-intercalated C_{60}.

III. SR-UPS OF $Yb_{2.75}C_{60}$

A. Experiment

The sample preparation procedure is analogous with that described in Sec. II except that the sample was characterized by the XPS measurements. When the C 1*s* movement towards lower binding energy reached 0.5 eV, we changed the spectrometry mode from XPS to UPS. The movement of 0.5 eV is the XPS characterization of phase-pure $Yb_{2.75}C_{60}$.[8,26,32] Six different photon energies from 18.0 eV to 45.0 eV were adopted to measure the electronic density of states near the Fermi level.

B. Results and discussions

The SR-UPS results of $Yb_{2.75}C_{60}$ with varying photon energies are shown in Fig. 3. The spectral line with the incident photon energy of 21.0 eV is much analogous with that[8] measured for $Yb_{2.75}C_{60}$ by using the He I radiation.

Line shape varies greatly with different incident photon energies in Fig. 3. After a set of datum as Fig. 3 was acquired, we repeatedly measured all the six UPS lines once again and obtained the same results. Thus the drastic variations in Fig. 3 are not due to the experimental error or oxidization. The only possible reason for the shape variation is the photoionization cross section effect. Although the calculated results for atoms[28] exhibited the photoionization cross section increases for Yb 4*f* states and decreases for C 2*p* states within the photon energy range of this work, we could not anticipate such drastic line variations as in Fig. 3 before the SR-UPS measurements because of the photoionization cross section oscillation[36] of the HOMO and HOMO-1 bands of C_{60}. In the following, we will deduce quantitatively the component contributions to the spectral line of $Yb_{2.75}C_{60}$. The components include the C 2*p*-derived LUMO, HOMO, HOMO-1 bands, and the Yb $4f_{7/2}$ and $4f_{5/2}$ core levels.

We first subtracted the HOMO-2 contribution to the higher binding energy parts of the spectral lines by the exponent-type extrapolation, as in Ref. 34 The resulting spectral lines are shown with the triangle-linked lines in Fig. 4 (only the two spectral lines recorded with the photon energies of 21.0 eV and 35.0 eV are given as representative). Then we simulated the components with Gaussian-type lines

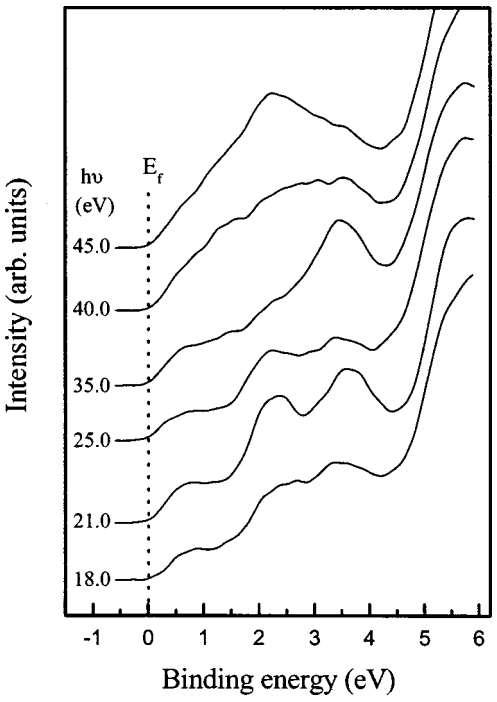

FIG. 3. SR-UPS of $Yb_{2.75}C_{60}$ with varying incident photon energies.

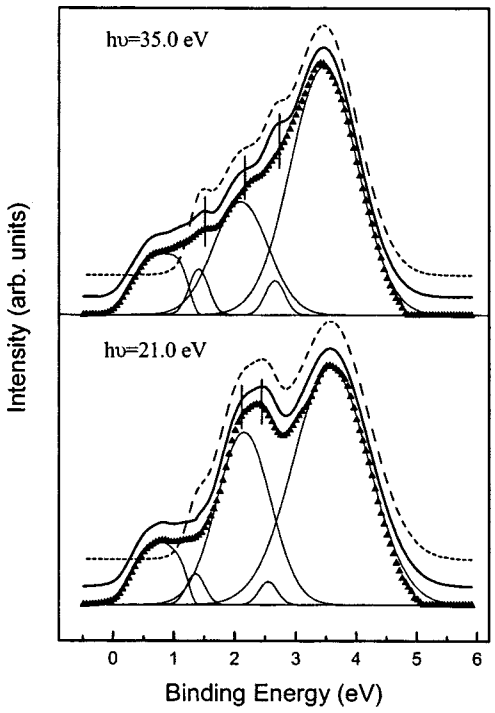

FIG. 4. Schematic representation of the determination of component contributions to the spectral lines. The five components, from lower binding energy to higher binding energy, are LUMO, $4f_{7/2}$, HOMO, $4f_{5/2}$ and HOMO-1 states. The components are simulated by Gaussian lines except the LUMO feature. The short vertical lines indicate the fine structures of the experimental lines can be reproduced by the simulation. The dashed lines represent the simulated sum of the $4f_{7/2}$, HOMO, $4f_{5/2}$, and HOMO-1 components. The triangle-linked lines are the experimental data, and the solid bold line represents the ultimately simulated result. The peak positions are ~1.40, ~2.13, ~2.65, and ~3.4 eV for $4f_{7/2}$, HOMO, $4f_{5/2}$, and HOMO-1, respectively.

except the LUMO band. The line shape of the LUMO feature remarkably departs from Gaussian shape due to the strong correlation and the possible hybridization effects.[27] We will obtain the LUMO component by subtracting the rest components, which will be obtained by a simulating process, from the experimental spectral line.

The quantitative contributions of the components are obtained by the least-square simulation method. The simulation, as schematically shown in Fig. 4, is carried out only for the parts with binding energies larger than the peak position of $4f_{7/2}$ because the LUMO feature cannot be simulated by the Gaussian-type line, as mentioned above.

The adjustable parameters in the simulation include peak positions, full widths at half-maximum (FWHMs) and peak heights. The peak height of $4f_{5/2}$ is fixed to be $3/4$ times that of $4f_{7/2}$, and the FWHMs for $4f_{7/2}$ and $4f_{5/2}$ are fixed to be the same to reduce the number of the adjustable parameters. We further imposed some constraints to the peak positions. In principle, we kept the peak positions unchanged for the spectral lines acquired with different incident phonon energies. We merely allowed the peak positions to vary within the range of ±0.05 eV to compensate for the experimental uncertainties. The starting values for the HOMO and HOMO-1 positions in the simulation process can be easily and rather accurately read from the lower three spectral lines in Fig. 3. The starting values for the Yb $4f$ positions are referenced to metal Yb (Ref. 8) and the XPS result of $Yb_{2.75}C_{60}$.[32] Thus, the adjustable parameters about the peak positions are mainly based on the experimental data, rather than indeed adjustable. The values that can make the simulated lines fit the experimental ones fairly well are 1.40(±0.04) eV, 2.13(±0.02) eV, 2.65(±0.05) eV, and 3.4(±0.03) eV for $4f_{7/2}$, HOMO, $4f_{5/2}$, and HOMO-1, respectively. The numbers in the parentheses are the scattering of the peak positions for the six spectral lines in Fig. 3, which are within the experimental uncertainty. The actual adjustable parameters are peak widths and heights. The starting values of the peak widths are referenced to metal Yb (Ref. 8) ($4f$ states) and Rb_3C_{60} (Ref. 34) (HOMO and HOMO-1). The simulated results of peak widths are slightly larger for the spectral lines measured with higher photon energies as compared to that for the spectral lines recorded with lower photon energies. For examples, the HOMO feature has FWHMs of 0.54 eV, 0.56 eV, and 0.62 eV for the spectral lines with the incident photon energy of 21.0 eV, 35.0 eV, and 45.0 eV. The FWHM variation coincides with the resolution variation of the spectrometry with varying photon energies.

The dashed line in Fig. 4 is the simulated result. It is the sum of the $4f_{7/2}$, HOMO, $4f_{5/2}$, and HOMO-1 components. The LUMO band is then obtained by subtracting the dashed line from the experimental line (represented by the triangle-linked line). This procedure should bring out error to the simulation if the $4f_{7/2}$ feature superposes on the LUMO feature too much. Fortunately, the LUMO band generally has a bandwidth less than ~1.3 eV in the UPS measurements as

has been revealed in the alkali and alkaline-earth fullerides. The $4f_{7/2}$ feature has a binding energy no less than 1.3 eV in $Yb_{2.75}C_{60}$. Only part of the $4f_{7/2}$ feature whose binding energy is less than the peak position (~1.4 eV, see the above paragraph) superposes on the LUMO band. Thus the superposition of the LUMO and $4f_{7/2}$ features does not affect the precision of the simulation to the part with binding energies larger than the peak position of $4f_{7/2}$. The resulting LUMO band is also rationality.

In Fig. 4, even some fine structures of the experimental data can be reproduced by the simulation. The fairly good simulation process makes us believe that Fig. 4 successfully discriminates the valence bands from the $4f$ core levels.

For all the spectral lines recorded with six different phonon energies, we schematically show in Fig. 5 the ratios between the spectral area of each component and the total area of the experimental line. The $4f$ contributions are less than 2.5% below 25.0 eV in Fig. 5. The UPS measurements with photon energies less than 25.0 eV thus reflect mainly the valence bands of $Yb_{2.75}C_{60}$. With the photon energy of 40.0 eV, the contribution of the $4f$ features increases by ~3 times. Taking into account that the peak widths of the $4f$ core levels are much narrower than that of the valence bands, their peak heights increase more remarkably. The $4f$ states locate just at the hollow regions of the density of states of the valence bands. So, the contributions of the $4f$ states drastically change the shape of the UPS line recorded with high photon energies. However, the valence band of $Yb_{2.75}C_{60}$ can be deduced by utilizing the synchrotron radiation in the photoemission measurements, whether the $4f$ contributions are minor or significant.

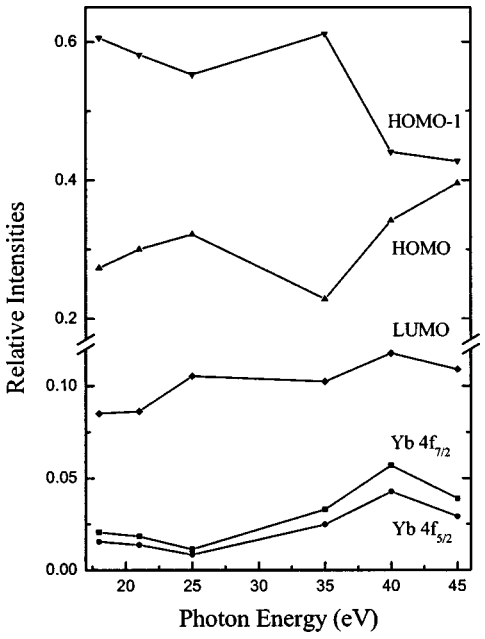

FIG. 5. Relative intensities, i.e., the area ratio between each component and the total area of the experimental lines, for the spectral lines recorded with different photon energies.

IV. CONCLUSIONS

Valence evolution of Yb-intercalated C_{60} film demonstrates that the superconducting Yb fulleride is semiconducting at room temperature, whatever its stoichiometry is. Based on this observation, we speculate that interesting phenomena such as electronic or structural phase transitions, besides the superconducting transition, should be observed in Yb-C_{60} compounds at low temperatures. Besides $Yb_{2.75}C_{60}$, other phases seem to exist in the Yb-intercalated C_{60} materials with the LUMO+1 band filled. The valence band of $Yb_{2.75}C_{60}$ is extracted quantitatively from the $4f$-core-level-superposed photoemission data by utilizing the synchrotron radiation.

ACKNOWLEDGMENTS

This work is supported by Beijing Synchrotron Radiation Facility and the National Natural Science Foundation of China under Contract No. 10074053.

*Corresponding author: phylihn@public.zju.edu.cn

[1] A. F. Hebard, M. J. Rosseinsky, R. C. Haddon, D. W. Murphy, S. H. Glarum, T. T. M. Palstra, A. P. Ramirez, and A. R. Kortan, Nature (London) **350**, 600 (1991).

[2] A. R. Kortan, N. Kopylov, S. Glarum, E. M. Gyorgy, A. P. Ramirez, R. M. Fleming, F. A. Thiel, and R. C. Haddon, Nature (London) **355**, 529 (1992).

[3] E. Özdas, A. R. Kortan, N. Kopylov, A. P. Ramirez, T. Siegrist, K. M. Rabe, H. E. Bair, S. Schuppler, and P. H. Citrin, Nature (London) **375**, 126 (1995).

[4] X. H. Chen and G. Roth, Phys. Rev. B **52**, 15 534 (1995).

[5] I. Margiolaki, S. Margadonna, K. Prassides, T. Hansen, K. Ishii, and H. Suematsu, J. Am. Chem. Soc. **124**, 11288 (2002).

[6] K. Ishii, A. Fujiwara, H. Suematsu, and Y. Kubozono, Phys. Rev. B **65**, 134431 (2002).

[7] T. Takenobu, D. H. Chi, S. Margadonna, K. Prassides, Y. Kubozono, A. N. Fitch, K. Kato, and Y. Iwasa, J. Am. Chem. Soc. **125**, 1897 (2003).

[8] Hongnian Li, Shaolong He, Hanjie Zhang, Bin Lu, Shining Bao, Haiyang Li, Pimo He, and Yabo Xu, Phys. Rev. B **68**, 165417 (2003).

[9] M. J. Rosseinsky, A. P. Ramirez, S. H. Glarum, D. W. Murphy, R. C. Haddon, A. F. Hebard, T. T. M. Palstra, A. R. Kortan, S. M. Zahurak, and A. V. Makhija, Phys. Rev. Lett. **66**, 2830 (1991).

[10] A. Goldoni, L. Sangaletti, S. L. Friedmann, Z.-X. Shen, M. Peloi, F. Parmigiani, G. Comelli, and G. Paolucci, J. Chem. Phys. **113**, 8266 (2000).

[11] R. Hesper, L. H. Tjeng, A. Heeres, and G. A. Sawatzky, Phys. Rev. B **62**, 16 046 (2000).

[12] T. Takahashi, T. Morikawa, S. Hasegawa, K. Kamiya, H. Fujimoto, S. Hino, K. Seki, H. Katayama-Yoshida, H. Inokuchi, K. Kikuchi, S. Suzuki, K. Ikemoto, and Y. Achiba, Physica C **190**, 205 (1992).

[13] Chun Gu, B. W. Veal, R. Liu, A. P. Paulikas, P. Kostic, H. Ding,

K. Gofron, J. C. Campuzano, J. A. Schlueter, H. H. Wang, U. Geiser, and J. M. Williams, Phys. Rev. B **50**, 16 566 (1994).
[14] M. Baenitz, M. Heinze, K. Lüders, H. Werner, R. Schlögl, M. Weiden, G. Spam, and F. Steglich, Solid State Commun. **96**, 539 (1995).
[15] B. Gogia, K. Kordatos, H. Suematsu, K. Tanigaki, and K. Prassides, Phys. Rev. B **58**, 1077 (1998).
[16] G. K. Wertheim, D. N. E. Buchanan, and J. E. Rowe, Science **258**, 1638 (1992).
[17] M. Knupfer, F. Stepniak, and J. H. Weaver, Phys. Rev. B **49**, 7620 (1994).
[18] S. Saito and A. Oshiyama, J. Phys. Chem. Solids **54**, 1759 (1993).
[19] G. K. Wertheim and D. N. E. Buchanan, J. Phys. Chem. Solids **56**, 745 (1995).
[20] R. C. Haddon, G. P. Kochanski, A. F. Hebard, A. T. Fiory, and R. C. Morris, Science **258**, 1636 (1992).
[21] R. C. Haddon, G. P. Kochanski, A. F. Hebard, A. T. Fiory, R. C. Morris, and A. S. Perel, Chem. Phys. Lett. **203**, 433 (1993).
[22] Y. Chen, D. M. Poirier, M. B. Jost, C. Gu, T. R. Ohno, J. L. Martins, J. H. Weaver, L. P. F. Chibante, and R. E. Smalley, Phys. Rev. B **46**, 7961 (1992).
[23] J. Takeuchi, K. Tanigaki, and B. Gogia, in *Nanonetwork Materials: Fullerenes, Nanotubes, and Related Systems*, edited by S. Saito, T. Ando, Y. Iwasa, K. Kikuchi, M. Kobayashi, and Y. Saito, AIP Conf. Proc. No. 590 (AIP, New York, 2001), p. 361.
[24] J. Arvanitidis, Konstantinos Papagelis, Serena Margadonna, Kosmas Prassides, and Andrew N. Fitch, Nature (London) **425**, 599 (2003).
[25] D. Claves and A. Hamwi, Solid State Commun. **113**, 357 (2000).
[26] Shaolong He, Hongnian Li, Haiyang Li, Hanjie Zhang, Bin Lu, Pimo He, Shining Bao, and Yabo Xu, Acta Phys. Sin. **53**, 915 (2004) (in Chinese).
[27] P. H. Citrin, E. Özdas, S. Schuppler, A. R. Kortan, and K. B. Lyons, Phys. Rev. B **56**, 5213 (1997).
[28] J. J. Yeh and I. Lindau, *Atomic Subshell Photoionization Cross Section and Asymmetry Parameters: $1 \leqslant Z \leqslant 103$* (Academic, New York, 1985), pp. 7–11.
[29] Hongnian Li, Yabo Xu, Jianhua Zhang, Peimo He, Haiyang Li, Taiquan Wu, and Shining Bao, Prog. Nat. Sci. **11**, 427 (2001).
[30] T. Durakiewicz, S. Halas, A. Arko, J. J. Joyce, and D. P. Moore, Phys. Rev. B **64**, 045101 (2001).
[31] H. N. Li, X. X. Wang, S. L. He, H. J. Zhang, H. Y. Li, and S. N. Bao, Chin. Phys. **13**, 1941 (2004).
[32] T. R. Ohno, G. H. Kroll, J. H. Weaver, L. P. F. Chibante, and R. E. Smalley, Phys. Rev. B **46**, 10 437 (1992).
[33] L. H. Tjeng, R. Hesper, A. C. L. Heessels, A. Heeres, H. T. Jonkman, and G. A. Sawataky, Solid State Commun. **103**, 31 (1997).
[34] Hongnian Li, Kurash Ibrahim, Fenqin Liu, and Yabo Xu, Surf. Sci. **540**, L631 (2003).
[35] X.-W Cao, J.-M. Hao, X.-S. Wu, Y.-F. Wang, Y. Wu, J.-J. Liu, S.-F. Hu, and G.-X. Lan, Appl. Phys. A: Mater. Sci. Process. **70**, 223 (2000).
[36] C. Ton-That, A. G. Shard, S. Egger, V. R. Dhanak, and M. E. Welland, Phys. Rev. B **67**, 155415 (2003).